International Journal of Minerals, Metallurgy and Materials
Volume 19, Number 12, Dec 2012, Page 1100
DOI: 10.1007/s12613-012-0677-0

Texture evolution of Al-Mg-Li aeronautical alloys in in-situ tension

Zhong-wei Chen, Jing Zhao, and Shi-shun Li

State Key Laboratory of Solidification Processing, Northwestern Polytechnical University, Xi'an 710072, China

(Received: 13 March 2012; revised: 14 May 2012; accepted: 15 May 2012)

Abstract: Texture evolution in extruded and hot-rolled Al-Mg-Li aeronautical alloys during in-situ tension was investigated by using electron backscattered diffraction (EBSD). A field emission scanning electron microscope (FE-SEM) and a MICROTEST-5000 tensile stage were used to carry out in-situ tension tests and observations. The crystallographic texture of the extruded sample changed from weak cube texture {001}<100> to texture {018}<081> during tension fracture. However, strong Brass {110}<112> in the hot-rolled sample was modified into a mixture texture component of Brass {110}<112> and S {123}<634> during tension fracture. Texture evolution in the two samples during tension can be explained by the rotation of grain orientation.

Keywords: aluminum lithium alloys; textures; tensile testing; extrusion; hot rolling

[*This work was financially supported by the Innovation Fund of China Aerospace Science and Technology Corporation (2011), the Research Fund of the State Key Laboratory of Solidification Processing (No.42-QP-009), and the 111 Project of China (No.B08040).***]**

1. Introduction

Due to the excellent properties of low density, high specific strength, and high specific stiffness [1], as well as their good low-temperature performance, corrosion resistance, and outstanding super plastic performance [2-3], Al-Li alloys have become the most ideal low-density and high-strength structural material that is applicable for aeronautical industries and aerospace structural components such as fuel-storage cells [4].

As a widely used Al-Li alloy, Al-Mg-Li is characterized by a high elastic modulus and low density. Like other Al-Li alloys, after casting, the alloy is subjected to a considerable plastic deformation via extrusion or rolling at high temperature and subsequent heat treatment. These processes lead to the formation of some degree of crystallographic and morphological texture, which results in a considerable anisotropy of mechanical properties [5-6]. One possible reason is a higher degree of crystallographic texture and in particular a strong Brass {110}<112> component [7-8]. In addition to the strong crystallographic texture, the interaction between the particular precipitation and the crystallographic texture should be considered [9-10].

Texture analysis is powerful in investigating the microstructural evolution of materials after deformation and annealing. It provides information about the processing history of the materials. Ref. [8] shows that the presence of Li is not intrinsically responsible for the development of strong Brass components, and that the deformation temperature has a major influence on texture development. Texture evolution during accumulative roll bonding of Al-Li alloy is investigated up to three passes, the texture components after the first pass cannot be characterized as the ideal shear texture components and the decrease of texture intensity along with the evolution of ideal FCC rolling texture components can be correlated well with the additional strain imposed during subsequent deformation [11].

Although numerous papers dealing with textures in Al-Li alloys have been published since the late 1980s, the anisotropy of mechanical properties due to texture evolution

Corresponding author: Zhong-wei Chen E-mail: chzw@nwpu.edu.cn

seems to be well understood [4-14], and texture evolution of fracture has not been well explored and still should be investigated further [15]. It would greatly contribute to the understanding and control of texture-induced directionality of stretch formability, which is known to be of significant concern in forming operations and structural design.

Textures of Al-Mg-Li alloys for some aeronautical and aerospace structural components could be changed during service and then lead to fracture or failure. In this research, texture evolution in extruded samples and hot-rolled samples was studied by using electron backscattered diffraction (EBSD) and an in-situ tensile stage, which is installed in field emission scanning electron microscopy (FE-SEM).

2. Experimental

Samples used in this experiment are 1420 extruded rods supplied by Southwest Aluminum Group Co., Ltd. of China and the chemical composition is shown in Table 1.

Table 1. Chemical composition of 1420 alloy

Mg / wt%	Li / wt%	Zr / wt%	Si / wt%	Fe / wt%	Cu / wt%	Ti / wt%	Na / wt%	H / cm^3 per 100 g	Al / wt%
5.25	2.13	0.11	0.025	0.08	0.005	<0.01	0.0005	0.53	Bal.

The samples were separated into two groups, one for heat treatment and the other for hot-rolling. On the one hand, the heat treatment process for the first group is as follows: firstly, the samples were held at 450°C for 20 h for homogenization treatment, then transferred to a salt-bath furnace for the solution treatment at 460°C for 45 min, and finally carried out aging treatment at 120°C for 12 h. On the other hand, for the second hot-rolled samples, they were hot rolled into 10 mm thick sheets at a rolling temperature of 460°C and a thickness reduction of 50% every pass.

The samples were machined to the final shape for in-situ tensile test as shown in Fig. 1. For the hot-rolled samples, the long edge is along the rolling direction. All tensile samples were ground and polished and finally etched on a Gatan 682 ion etching machine for EBSD mapping.

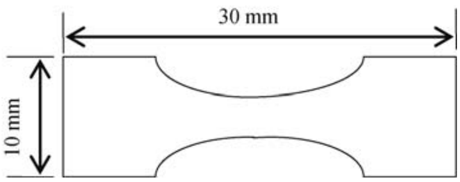

Fig. 1. Shape of tension samples.

The specimens were fixed on a MICROTEST-5000 tensile stage, which is installed in a Zeiss SUPRA55 FE-SEM to carry out in-situ tensile testing. Fig. 2 schematically shows the in-situ tensile stage in a vacuum chamber of a SEM. The tension speed was set at 0.005 mm·s^{-1}. With the tensile load rising, microcracks appeared and grew gradually, which lead to fracture of specimens finally.

EBSD samples were cut from the right area of tension specimens. EBSD tests were performed in a Zeiss SUPRA55 FE-SEM with HKL channel 5 with an acceleration voltage of 20 kV, a working distance of 23.6 mm, an aperture diameter of 60 μm, and a vacuum under 5×10^{-3} Pa.

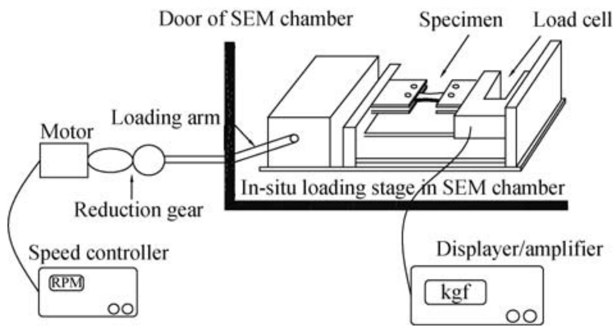

Fig. 2. Schematic diagram of an in-situ tensile stage in SEM.

3. Results

3.1. Texture evolution of extruded samples

Fig. 3 gives the pole figures of the {100}, {110}, and {111} planes from different areas of the extruded samples. In Fig. 3(a), an apparent black region in the centre of the {100} pole figure is observed, which indicates that the {100} planes have a sizable distribution density in the unstretched area. However, the orientation concentration region in the {110} and {111} pole figures is not observed, which indicates that the {110} and {111} planes are weak texture compared with the {100} planes. Therefore, it shows that, before tension, the {100} planes of most grains are parallel to X_0OY_0, which is the macroscopic surface of the sample.

In Fig. 3(b), much more black regions in the {100} polar figure of the stretched area are observed. At the same time, compared with the {100} polar figure of the unstretched area, the black regions are not only in the centre but also disperse throughout the figure in the {100} polar figure.

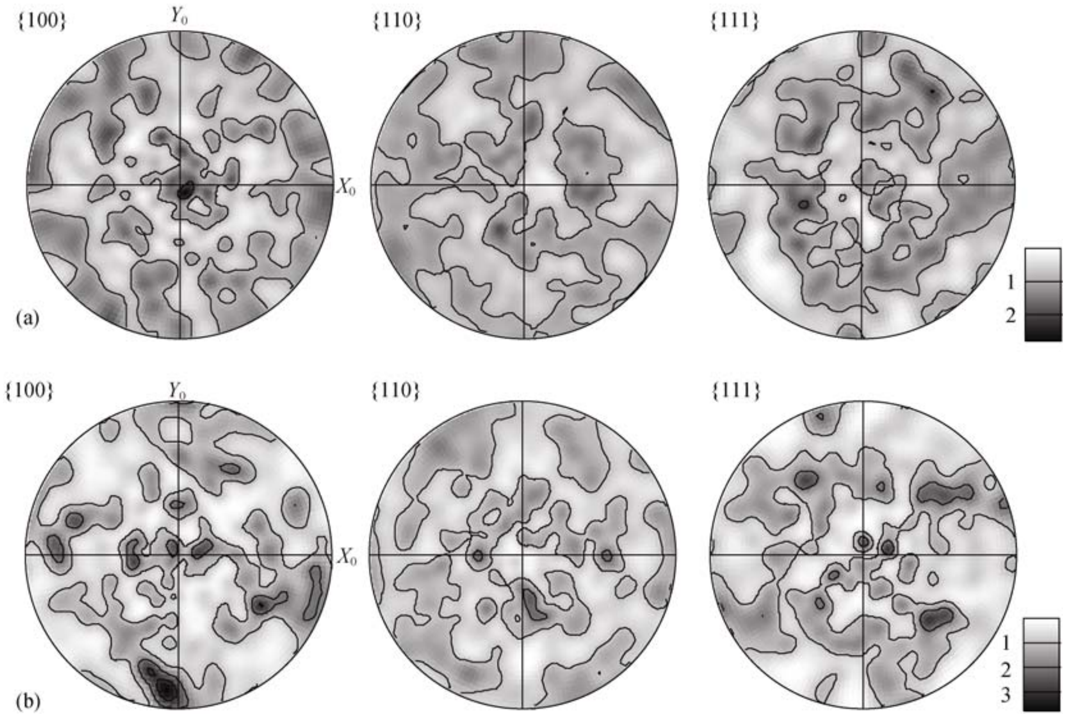

Fig. 3. Pole figures of extruded samples: (a) unstretched area; (b) stretched area.

Furthermore, the black regions in the {110} and {111} polar figures are also observed, which indicates that the grain orientation changes after tension and the base-plane {100} texture disappears. Comparing the {100} polar figure of stretched area with the standard {001} polar figure of cubic crystals, it could be concluded the existing of the approximate {001}<100> texture after tension.

To clarify the change of grain orientation during tension, the orientation distribution function (ODF) graph of the stretched area using the HKL EBSD post-processing software is shown in Fig. 4. From Fig. 4, Euler angles are calculated and some important orientation information in the stretched area is obtained; some textures as follows: {014}<041>, {160}<610>, and {018}<081>. Therefore, the {104}, {106}, and {108} polar figures of the stretched area are shown in Fig. 5. It shows that the grain orientation has a tendency of concentrating towards the central, top, and down, and lateral poles. Comparing the polar figure with the standard {001} polar figure of cubic crystals, it is found that there exists the {018}<081> texture that is approximate to the {001}<100> texture in the stretched area.

3.2. Texture evolution of hot-rolled sheets

Fig. 6 gives the polar figures of the {100}, {110}, and {111} planes from different areas of the hot-rolled samples, respectively. In Fig. 6(a), as the black spots concentrate on particular positions, it shows that the polar figures of the hot-rolled samples have a strong regularity. Comparing the {110} polar figure in Fig. 6(a) with the standard {110} polar figure of cubic crystals, the Brass {110}<112> texture is found in the sample. After hot rolling, the Brass texture formed in the sample results in the {110} plane being parallel to the roll plane, i.e., the sample's X_0OY_0 plane, but the <112> parallel to the rolling direction, i.e., the X_0 direction.

In Fig. 6(b), an obvious change of the Brass texture {110}<112> in the stretched area is not observed, and it indicates that the Brass texture is strong under this rolling condition.

ODF series sections are used to verify the texture in the stretched and unstressed areas. Fig. 7 shows the ODF of the hot-rolled sheets in the unstretched (Fig. 7(a)) and stretched areas (Fig. 7(b)). By comparing with the standards and computing the Euler angles, it is found that the texture existing in the unstretched area is {110}<112>, and the texture in the stretched area is {110}<112> and {123}<634>, indicating that there comes the texture S {123}<634> in the stretched area.

4. Discussion

For an extruded sample, before tension, the base-plane {100} of grains is parallel to X_0OY_0 (Fig. 8), which is the macroscopic surface of the sample. Fig. 8 shows the schematic program of grain orientation before tension, where X_0

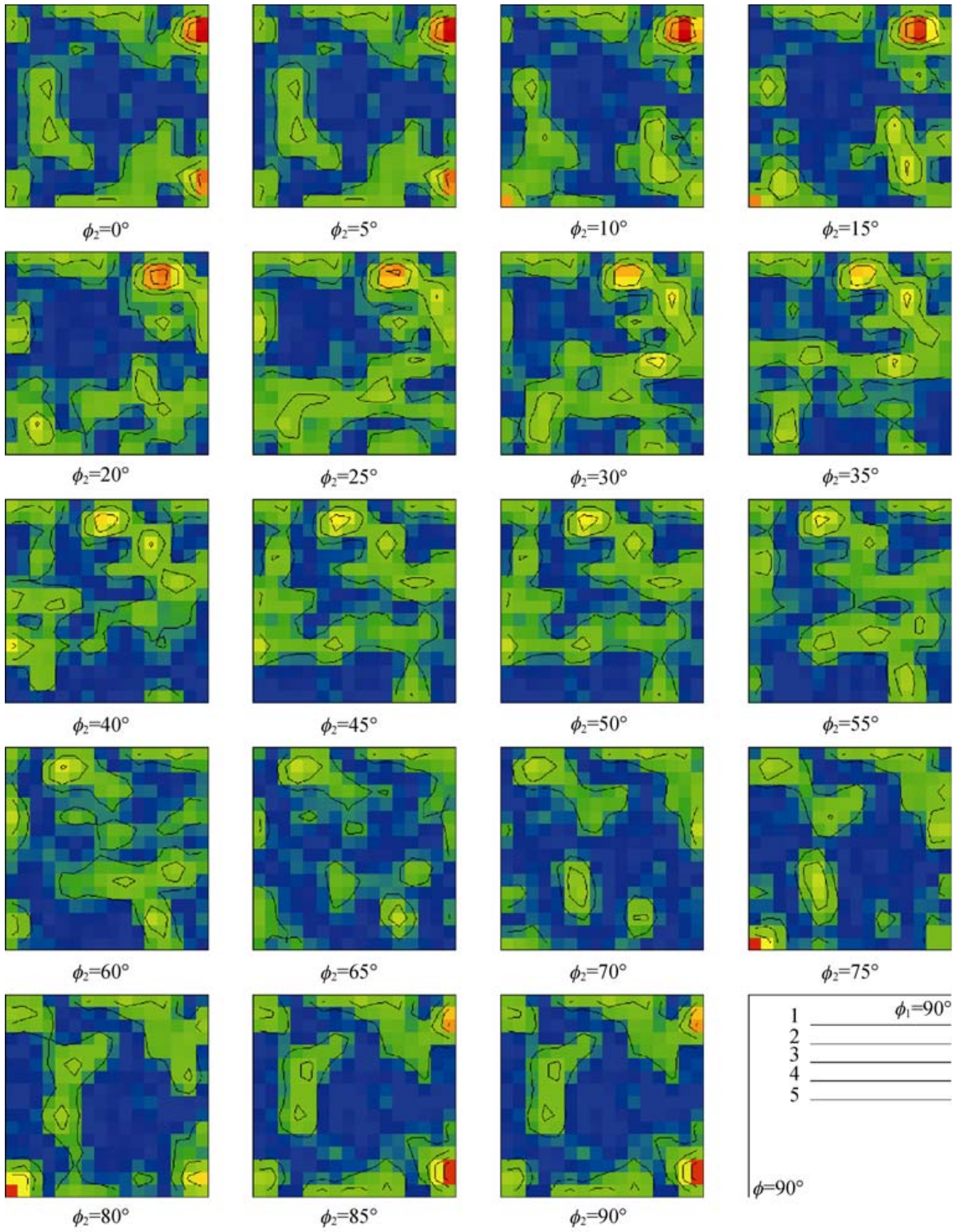

Fig. 4. ODF of the stretched area in extruded samples.

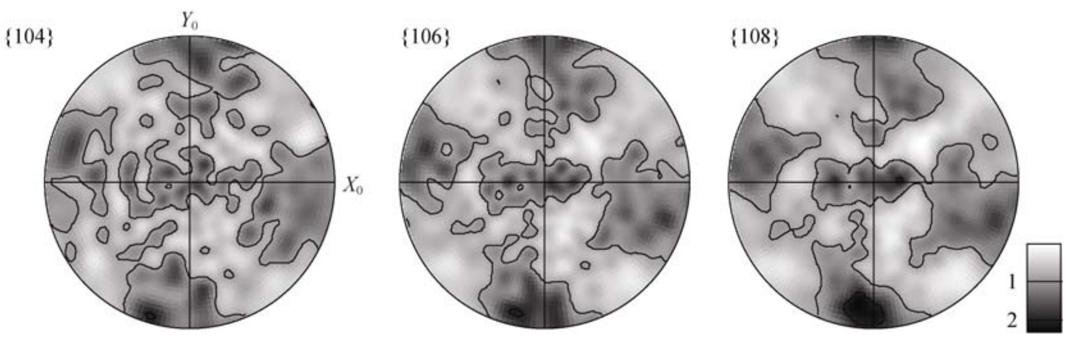

Fig. 5. Pole figures of the stretched area in extruded samples.

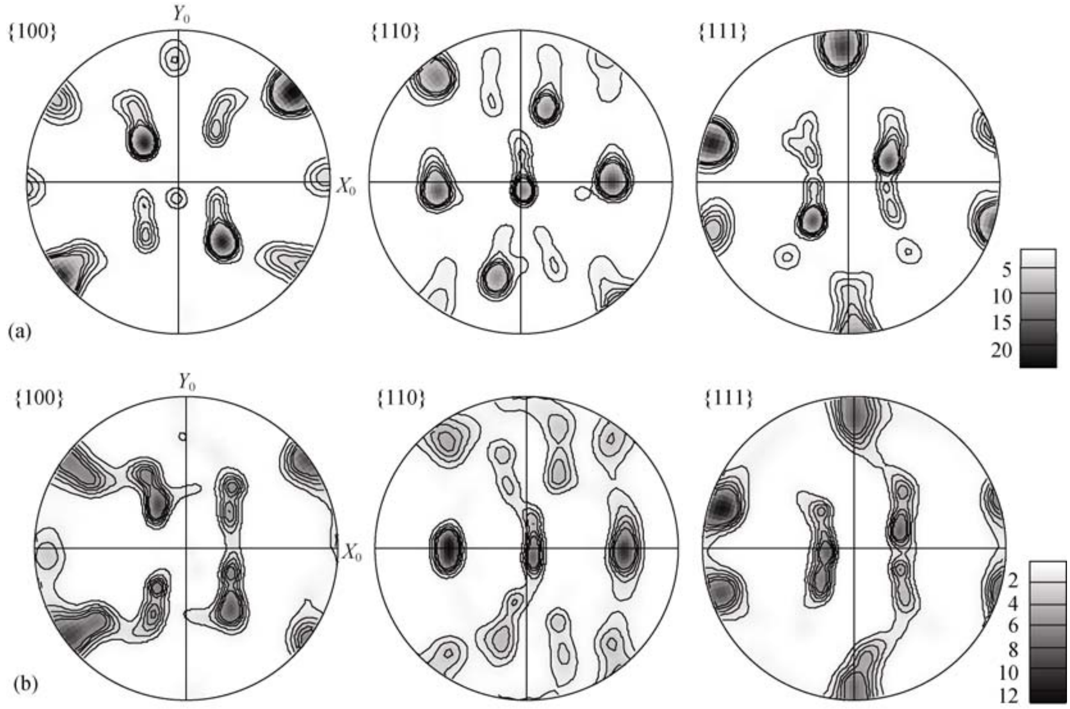

Fig. 6. Pole figures of hot-rolled sheets: (a) unstretched area; (b) stretched area.

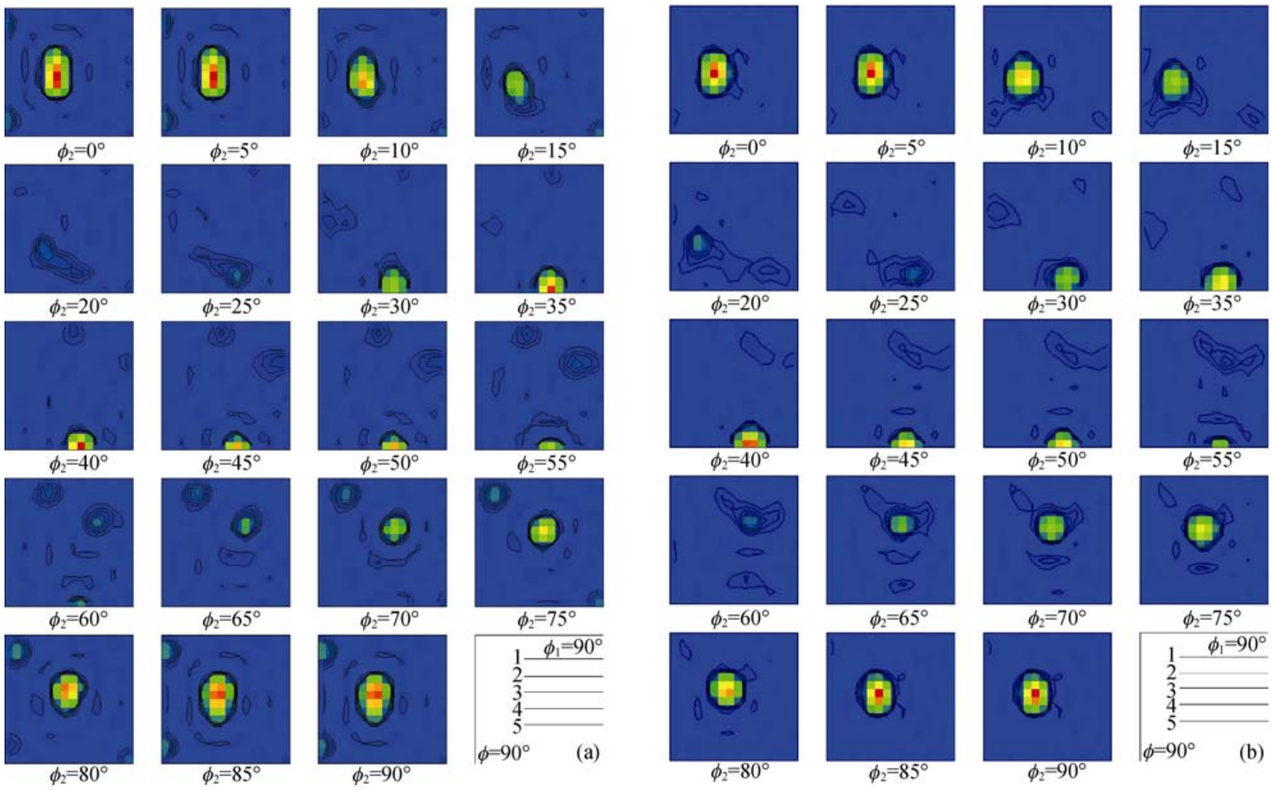

Fig. 7. ODF of hot-rolled sheets in the unstretched area (a) and the stretched area (b).

is parallel to the stretching direction and Z_0 is parallel to the normal direction of the sample surface. However, the grain distribution of the X_0 direction is not exactly the same as that of the Y_0 direction. Inverse polar figures (IPF) of different areas are shown in Fig. 9.

From Figs. 9(a) and 9(b), before tension, the normal direction of most grains' {001} planes is parallel to the Z_0 axis, but it is parallel to the Y_0 axis after tension. It indicates that

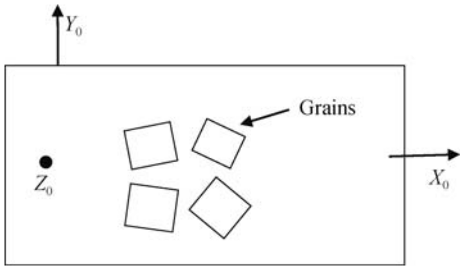

Fig. 8. Schematic program of grain orientation before tension (X_0-stretching direction).

the grains rotate around the [001] and [010] zone axis in the tension process, respectively. As a result, the {001} planes of most grains are perpendicular to the Y_0 axis and exhibit a certain angle with the X_0 and Z_0 axes. Fig. 10 illustrates the rotation of grain orientation in the tension process (Figs. 10(a) and 10(b)) and after the tension (Figs. 10(c) and 10(d)). Due to insufficient rotation around the [010] zone axis, the grains obtain the orientation that is approximate to the {001}<100> texture.

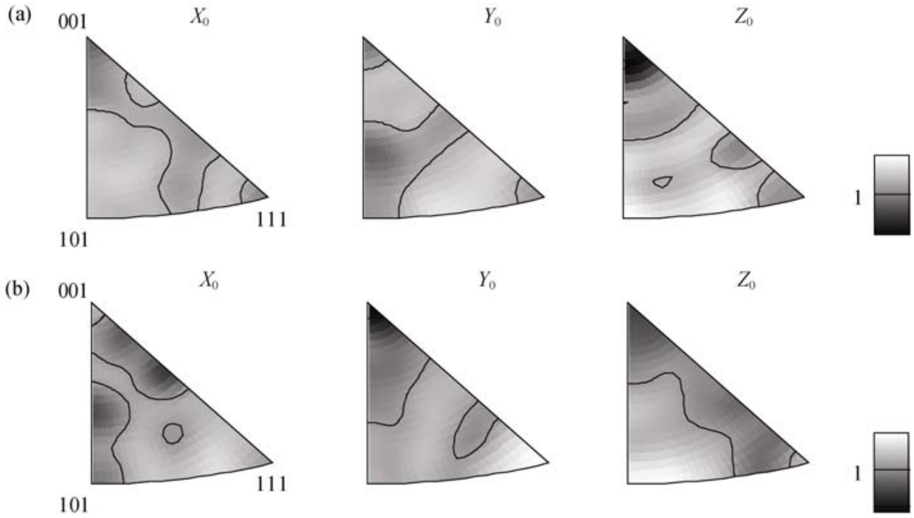

Fig. 9. IPF of different zones in the extruded sample: (a) unstretched area and (b) stretched area.

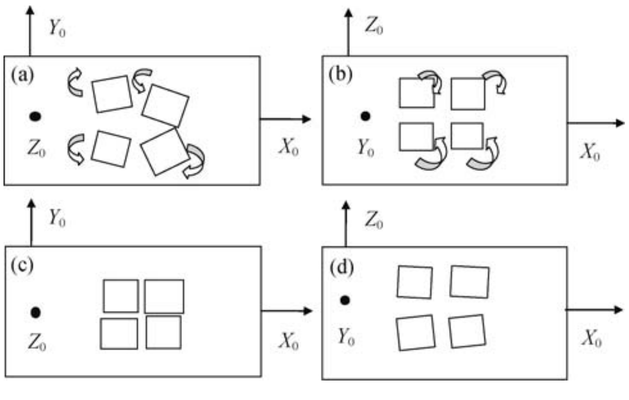

Fig. 10. Rotations of grain orientation in the tension process ((a) and (b)) and after the tension ((c) and (d)) (X_0-stretching direction).

Generally, under the condition of relatively large rolling deformation, some strong deformation textures including the Brass texture {110}<112>, S texture {123}<634>, copper texture {112}<111>, cube texture {100}<001>, and Goss texture {110}<001> [16] will be formed in cubic materials. Strong textures cannot be changed obviously in the tension process. For hot-rolled sheet samples in this study, strong Brass {110}<112> was modified into a mixture texture component of Brass {110}<112> and S {123}<634> in tension fracture.

In fact, calculation results from the ODF graphs show that, in the unstretched area, the Euler angles, a type of texture, are 58.4°, 31.5°, and 65.0°, respectively, somewhat approximating to the S texture. By comparison, the Euler angles of the texture in the stretched area are 58.0°, 35.5°, and 65.0°, which are more approximate to those of S texture of 60.0°, 35.0°, and 65.0°. It indicated that there exists S texture in the stretched area. Therefore, for hot-rolled sheets, due to a bigger rolling deformation, most grains in the stretched area rotate 4.0° more than those in the unstretched area during the tension process.

5. Conclusions

(1) The crystallographic texture of extruded samples was changed from weak cube texture {001}<100> to texture {018}<081> in tension fracture.

(2) Strong Brass texture {110}<112> in hot-rolled sam-

ples was modified into a mixture texture component of Brass {110}<112> and S {123}<634> in tension fracture.

(3) Texture evolution in the two samples in tension could result from the rotation of grain orientation.

References

[1] H. Kaya, E. Çadırl, and M. Gündüz, Directional cellular growth of Al-2 wt% Li bulk samples, *Appl. Phys. A*, 94(2009), No.1, p.155.

[2] L. Meng and X.L. Zheng, Overview of the effects of impurities and rare earth elements in Al-Li alloys, *Mater. Sci. Eng. A*, 237(1997), No.1, p.109.

[3] Y. Xun, M.J. Tan, and K.M. Liew, EBSD characterization of cavitation during superplastic deformation of Al-Li alloy, *J. Mater. Process. Technol.*, 162-163(2005), p.429.

[4] A. Steuwer, M. Dumont, J. Altenkirch, S. Birosca, A. Deschamps, P.B. Prangnell, and P.J. Withers, A combined approach to microstructure mapping of an Al-Li AA2199 friction stir weld, *Acta Mater.*, 59(2011), No.8, p.3002.

[5] Ł. Ciupiński, J. Mizera, and K.J. Kurzydłowski, Quantitative description of the morphologic texture in an Al-Li alloy, *Mater. Charact.*, 46(2001), No.5, p.359.

[6] L.Y. Ye, X.M. Zhang, Y.W. Liu, and J.G. Tang, Effects of temperatures on rolling failure and grain refinement of 01420 Al-Li alloy, *Rare Met. Mater. Eng.*, 37(2007), No.8, p.1431.

[7] K.V. Jata, S. Panchanadeeswaran, and A.K.Vasudevan, Evolution of texture, microstructure and mechanical property anisotropy in an Al-Li-Cu alloy, *Mater. Sci. Eng. A*, 257(1998), No.1, p.37.

[8] Q. Contrepois, C. Maurice, and J.H. Driver, Hot rolling textures of Al-Cu-Li and Al-Zn-Mg-Cu aeronautical alloys: experiments and simulations to high strains, *Mater. Sci. Eng. A*, 527(2010), No.27-28, p.7305.

[9] N.J. Kim and E.W. Lee, Effect of T_1 precipitate on the anisotropy of Al-Li alloy 2090, *Acta Metall. Mater.*, 41(1993), No.3, p.941.

[10] Y.Z. Shen, K.H. Oh, and D.N. Lee, Serrated flow behavior in 2090 Al-Li alloy influenced by texture and microstructure, *Mater. Sci. Eng. A*, 435-436(2006), p.343.

[11] S.G. Chowdhury, A. Dutta, B. Ravikumar, and A. Kumar, Textural evolution during accumulative roll bonding of an Al-Li alloy, *Mater. Sci. Eng. A*, 428(2006), No.1-2, p.351.

[12] E. Romhanji, D. Mitlin, and V. Radmilovic, Deformation pattern and strain hardening in a highly textured 8090 Al-Li alloy sheet, *Mater. Sci. Eng. A*, 291(2000), No.1-2, p.160.

[13] S.C. Hogg, I.G. Palmer, L.G. Thomas, and P.S. Grant, Processing, microstructure and property aspects of a spraycast Al-Mg-Li-Zr alloy, *Acta Mater.*, 55(2007), No.6, p.1885.

[14] R.J. Rioja, Fabrication methods to manufacture isotropic Al-Li alloys and products for space and aerospace applications, *Mater. Sci. Eng. A*, 257(1998), No.1, p.100.

[15] W. Tayon, R. Crooks, M. Domack, J. Wagner, and A.A. Elmustafa, EBSD study of delamination fracture in Al-Li alloy 2090, *Exp. Mech.*, 50(2010), No.1, p.135.

[16] J. Mizera and J.H. Driver, Microtexture analysis of a hot deformed Al-2.3wt.%Li-0.1wt.%Zr alloy, *Mater. Sci. Eng. A*, 271(1999), No.1-2, p.334.